# Effects of Target Signal Shape and System Dynamics on Feedforward in Manual Control

Drop, Frank M.; Pool, Daan M.; van Paassen, Marinus M.; Mulder, Max; Bulthoff, Heinrich H.

**Important note**
To cite this publication, please use the final published version (if applicable).
Please check the document version above.

# Effects of Target Signal Shape and System Dynamics on Feedforward in Manual Control

Frank M. Drop, *Student member, IEEE,*  Daan M. Pool, *Member, IEEE,* Marinus (René) M. van Paassen, *Senior member, IEEE,* Max Mulder, Heinrich H. Bülthoff, *Member, IEEE*

*Abstract*—The human controller (HC) in manual control of a dynamical system often follows a visible and predictable reference path (target). The HC can adopt a control strategy combining closed-loop feedback and an open-loop feedforward response. The effects of the target signal waveform shape and the system dynamics on the human feedforward dynamics are still largely unknown, even for common, stable, vehicle-like dynamics. This paper studies the feedforward dynamics through computer model simulations and compares these to system identification results from human-in-the-loop experimental data. Two target waveform shapes are considered, constant velocity ramp segments and constant acceleration parabola segments. Furthermore, three representative vehicle-like system dynamics are considered: a single integrator, a second-order system, and a double integrator. The analyses show that the HC utilizes a combined feedforward/feedback control strategy for all dynamics with the parabola target, and for the single integrator and second-order system with the ramp target. The feedforward model parameters are, however, very different between the two target waveform shapes, illustrating the adaptability of the HC to task variables. Moreover, strong evidence of anticipatory control behavior in the HC is found for the parabola target signal. The HC anticipates the future course of the parabola target signal given extensive practice, reflected by *negative* feedforward time delay estimates.

## I. Introduction

MANUAL control of a dynamic system requires the human controller (HC) to efficiently steer the system along a certain target path while compensating for disturbances. An example is the manual control of an aircraft during turns or ascends and descends in the presence of turbulence. The HC uses all available sensory information and knowledge gained through prior experience, to optimize performance and reduce effort [1]. Automation and shared-control interfaces in aviation, and the advent thereof in the automotive sector [2], [3] demand a better understanding of high-level, goal-directed steering inputs in human feedforward control [4].

The majority of existing HC models, identified from experimental human-in-the-loop data, describe compensatory control behavior, where the HC acts as a closed-loop feedback controller [5]. Models of higher level control behavior, such as pursuit and preview control [6], commonly include a *feedforward* on the target [7]–[9], providing better tracking performance than pure feedback control [10]. These models were, however, not identified from experimental data.

Models of compensatory control have limited applicability, because realistic control tasks rarely induce a pure compensatory control strategy. These models do, however, reveal that HC behavior depends primarily on the system dynamics and the target and disturbance signal (the *forcing functions*) properties [11]. That is, the compensatory feedback equalization dynamics depend primarily on the system dynamics [12], and the quasi-linear model parameters depend primarily on the forcing functions [5], [13]. The effect of system dynamics and target signal properties on human feedforward control has received little attention and is still mostly unknown [14].

This paper investigates the adaptation of feedforward dynamics to the system dynamics and the target signal properties. Two main hypotheses were postulated in [10] and [15].

First, the ideal feedforward dynamics are equal to the inverse system dynamics [10] and the HC is expected to utilize similar dynamics. Wasicko *et al.* [10] indeed found evidence for a (sub-optimal) inversion of system dynamics in pursuit tasks. The deviations from the ideal dynamics likely stem from human limitations in perception, cognition, and action. Recent studies modeled these limitations by a gain, a low-pass filter, and a time delay [14], [16], [17], but they disagree on the exact model structure and order of the low-pass filter.

Second, it was stated that the utilization of feedforward is affected by the predictability of the target signal [5], [8], which is expected to depend on its waveform shape [15]. This hypothesis was, however, not experimentally investigated. Nevertheless, upon comparing the results of [10] and [14], a strong interaction between system dynamics and target signal shape indeed seems present. Ref. [10] investigated feedforward with "unpredictable" sum-of-sine targets and found little evidence of feedforward with a single integrator (SI), but strong evidence with a double integrator (DI). Ref. [14] used "predictable" ramp shaped targets and found the opposite: strong evidence for feedforward with an SI, but less conclusive evidence for a DI. However, objective metrics quantifying the predictability of the targets were not presented.

Recent advances in system identification [18] now allow for the investigation of feedforward control in realistic control tasks. To investigate the adaptation of manual feedforward control behavior to the target waveform shape and the system dynamics, we consider two realistic target waveform shapes and three classes of vehicle-like system dynamics. We will not explicitly investigate the predictability of the two targets, but rather focus on how the human feedforward dynamics adapt to different waveform shapes. We will consider constant velocity ramp segments, as used in [14], [16], [17], and compare

these to constant acceleration parabola segments. The parabola segments represent maneuvers in which the vehicle attitude is changed in minimum time, whilst keeping the vehicle accelerations within certain limits.

By far, the majority of vehicles under manual control are dynamically stable systems, either by design or through added augmentation systems, and can therefore be described by integrator or second-order system dynamics; sometimes by a double integrator [11]. While in very rare occasions HCs may be briefly (e.g., during hover in unaugmented helicopter flight) and unexpectedly (e.g., system malfunction) confronted with unstable dynamics, in such cases improving control performance through feedforward control will likely not play an important role, given the required emphasis on retaining stability. In this paper, we aim to study human behavior as it appears in the vast majority of control tasks, and therefore consider three stable, common, vehicle-like system dynamics, i.e., the easy-to-control SI, a second-order system, and the difficult-to-control DI.

The interaction between target waveform shape and system dynamics is investigated by means of an offline analysis with hypothesized HC models and a human-in-the-loop experiment. The offline analysis will investigate the potential performance improvement provided by a feedforward response as a function of target signal waveform shape, system dynamics, and model parameter values. Two complementary system identification and parameter estimation methods are used to analyze experimental human-in-the-loop data. A recently developed black-box ARX identification procedure, which is robust to false-positive feedforward identification, is used to identify HC dynamics [18]. A time-domain parameter estimation method [19], using HC models based on the ARX results, is used to obtain further insight in the correct model structure and to observe changes in control behavior.

The paper is structured as follows: Section II further introduces the control task under investigation. Section III introduces the HC model used in the offline analysis of Section IV. The human-in-the-loop experiment is described in Section V, the results of which are described in Section VI. The paper ends with a discussion and conclusions.

## II. CONTROL TASK

This paper focuses on human control behavior in a combined target-tracking and disturbance-rejection task, as shown in Fig 1. In this case an aircraft pitch attitude control task is shown. The HC controls the dynamic system $Y_c$ such that the
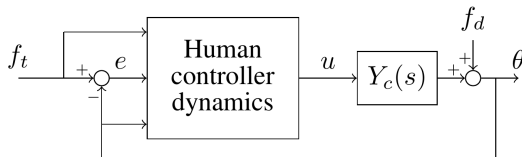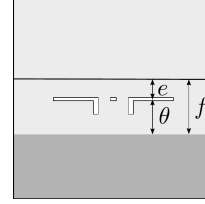

Fig. 2. Pursuit displays for pitch control. The display shows only the current values of the signals. No post or preview information is presented.

### A. System Dynamics $Y_c$

Three variations of $Y_c$ will be considered: the single integrator (SI) of (1), the second order system (S2D) of (2), and the double integrator (DI) of (3),

$$Y_c^{\text{SI}}(s) = K_c^{\text{SI}}/s \tag{1}$$

$$Y_c^{\text{S2D}}(s) = \frac{2K_c^{\text{S2D}}}{s\,(s+2)} \tag{2}$$

$$Y_c^{\text{DI}}(s) = K_c^{\text{DI}}/s^2 \tag{3}$$

With $K_c^{\text{SI}} = 1$, $K_c^{\text{S2D}} = 2.75$, and $K_c^{\text{DI}} = 5$.

### B. Target Signal $f_t$

Three variations of $f_t$ are considered: 1) a signal composed of constant velocity ramp (R) segments, 2) a signal composed of constant acceleration parabola (P) segments, and 3) a constant and zero target signal (Z), resulting in a pure disturbance-rejection task. The purely compensatory control behavior observed with the Z target is compared to the compensatory behavior observed simultaneously with feedforward with the R and P targets. Feedforward behavior can be investigated with the predictable R and P signals only, which are composed of several ramp and parabola segments of 3.75 and 7.5 s duration. Fig. 3 shows one individual ramp and parabola segment of 7.5 s and their first and second derivatives.


Fig. 1. Control scheme studied here. The HC can use target signal $f_t$, the system output $\theta$ and the error $e$ to generate the control signal $u$.

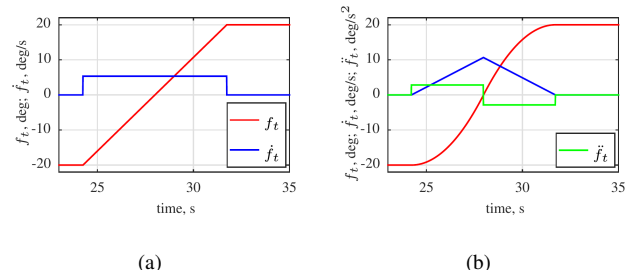error $e$ defined as $e = f_t - \theta$, remains as small as possible.


Fig. 3. Discrete target signal segments considered in this study. (a) Ramp. (b) Parabola.

The ramp signal velocity, Fig. 3(a), changes instantaneously from zero to 5.3 deg/s and back to zero, rendering an infinitely large second derivative at the ramp discontinuities. The parabola signal acceleration, Fig. 3(b), changes instantaneously thrice during a segment. First, it jumps from zero to 2.8 deg/s$^2$, causing the target velocity to increase linearly. Then, at exactly half the segment duration, the acceleration changes sign, causing the target velocity to decrease linearly, resulting in a waveform of two smoothly connected parabolas.

Each combination of system dynamics and a target signal will be referred to here with the syntax "$\{SI, S2D, DI\} - \{Z, R, P\}$". For example, SI-P designates the condition with single integrator dynamics and the parabola target signal.

## III. HC MODEL

We will first perform simulations with HC models to investigate the usefulness of a feedforward strategy and how this depends on the hypothesized limitations in the feedforward control action. Fig. 4 shows the structure of the HC model assumed for all three system dynamics, identical to the Inverse Feedforward Model (IFM) of [14]. The model consists of three components: 1) a feedforward path $Y_{p_t}$, 2) a feedback path $Y_{p_e}$, and 3) a model of the neuromuscular system $Y_{nms}$. Signal $n$ indicates remnant, accounting for non-linearities present in the HC, and is the residual of the control signal that is not modeled by the linear model.
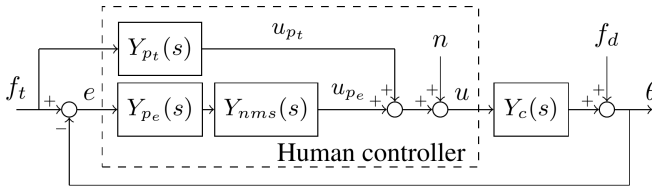


Fig. 4.  HC model block diagram.

The feedforward path $Y_{p_t}$ consists of a gain, inverse system dynamics [10], [14], [17], a low-pass filter, and a time delay:

$$Y_{p_t}(s) = K_{p_t} \frac{1}{Y_c(s)} \frac{1}{(T_I s + 1)^2} e^{-\tau_{p_t} s} \qquad (4)$$

The gain $K_{p_t}$ determines the overall strength of the feedforward response; setting $K_{p_t} = 0$ transforms the model to a pure feedback model. We will assume the theoretically ideal feedforward gain $K_{p_t}$ of 1, but note that previous studies have identified slightly lower values, $K_{p_t} \approx 0.9$ [14], [17].

Parameter $\tau_{p_t}$ captures the time delay present in the feedforward response, originating throughout the entire perception and action loop responding to the target signal. In our simulations and experimental data analyses we will also consider the possibility that $\tau_{p_t} < 0$, modeling *anticipatory* control behavior where the HC predicts the future course of the target. To simulate negative time delays, the feedforward path $Y_{p_t}$ responds to $f_t^*(t) = f_t(t+1)$ with the time delay $\tau_{p_t}^* = \tau_{p_t} + 1$, while the feedback path $Y_{p_e}$ responds to the error $e = f_t - \theta$, where $f_t$ is the unmodified target signal.

The low-pass filter parametrized by $T_I$ smoothens the ideal waveform of $u_{p_t}$ by filtering out high frequency content due

to the inversion of $f_t$ through $1/Y_c$, see Fig. 5. Note the similarity in waveform shape between $u_{p_t}$ in Fig. 5 and the first and second derivatives of $f_t$ in Fig. 3. For example, $u_{p_t}$ of SI-R is a smoothed step similar to the ramp's first derivative, and $u_{p_t}$ of DI-P is a smoothed doublet similar to the parabola's second derivative. The filter affects $u_{p_t}$ especially around discontinuities in the derivatives of $f_t$; here the filter removes the high frequent content of $u_{p_t}$.
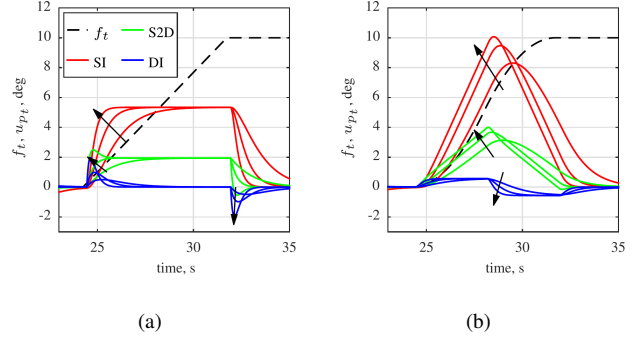


Fig. 5.  The feedforward control signal $u_{p_t}$ plotted for three different values of $T_I$ (0.2, 0.4, and 0.8 s). Arrows indicate evolution of signal shape as $T_I$ is reduced. The target $f_t$ is scaled by 0.25 and shifted up to start at 0 deg for clarity. (a) Ramp conditions. (b) Parabola conditions.

In [16] and [17], a first-order low-pass filter was assumed, but in [14] the filter was second-order. Similarly, two different assumptions regarding the position of the neuromuscular system in the model were made in [17] and [14]. In [17], the NMS acts on both the feedback and the feedforward path, whereas in [14] it acts only on the feedback path. The simulation results to be presented here are performed with the HC model and identified parameter values of [14] for consistency with this more recent work. The best model structure will be identified from experimental data through two identification methods.

The compensatory feedback component $Y_{p_e}$ of the combined feedforward-feedback HC model is modeled with a structure identical to McRuer's Extended Crossover Model [10], [11], [14], [17]. For second-order system dynamics (S2D and DI), the compensatory dynamics are described by:

$$Y_{p_e}(s) = K_{p_e}(T_L s + 1)e^{-\tau_{p_e} s} \qquad (5)$$

For the SI the lead time $T_L$ is zero.

The neuromuscular system (NMS) is commonly modeled as a mass-spring-damper system [11], [20]:

$$Y_{nms}(s) = \frac{\omega_{nms}^2}{s^2 + 2\zeta_{nms}\omega_{nms}s + \omega_{nms}^2} \qquad (6)$$

The HC model parameter values (Table I) are taken from [14] for the fastest of the two ramp targets (4 deg/s); these are closest to the ramp rate considered here (5.3 deg/s, Fig. 3(a)). The same values are used for the parabola in the following performance simulation analysis, to obtain a fair comparison.

## IV. PERFORMANCE SIMULATIONS

We hypothesize that the utilization of a feedforward control strategy by the HC depends on the potential performance improvement (PI) that the additional feedforward path delivers

TABLE I
HC MODEL PARAMETER VALUES USED IN SIMULATIONS

| | $K_{p_t}$ | $T_I$ | $\tau_{p_t}$ | $K_{p_e}$ | $T_L$ | $\tau_{p_e}$ | $\omega_{\text{nms}}$ | $\zeta_{\text{nms}}$ |
|---|---|---|---|---|---|---|---|---|
| | - | s | s | - | s | s | rad/s | - |
| SI | 1 | 0.25 | 0.22 | 1.55 | - | 0.19 | 14 | 0.22 |
| S2D | 1 | 0.25 | 0.35 | 0.75 | 0.4 | 0.24 | 10.1 | 0.35 |
| DI | 1 | 0.32 | 0.45 | 0.25 | 1.2 | 0.23 | 9.5 | 0.28 |

TABLE II
DISTURBANCE SIGNAL COMPONENTS

| $n_{f_d}$ | $A_{f_d}$, deg | $\phi_{f_d}$, rad | $n_{f_d}$ | $A_{f_d}$, deg | $\phi_{f_d}$, rad |
|---|---|---|---|---|---|
| 3 | 0.7828 | 1.2690 | 71 | 0.0525 | 0.3656 |
| 4 | 0.7637 | 2.6766 | 72 | 0.0515 | 4.8493 |
| 11 | 0.5597 | 4.5225 | 101 | 0.0328 | 0.9056 |
| 12 | 0.5290 | 1.1222 | 102 | 0.0325 | 4.4812 |
| 23 | 0.2788 | 4.1590 | 137 | 0.0238 | 1.4743 |
| 24 | 0.2640 | 1.6998 | 138 | 0.0236 | 5.8833 |
| 37 | 0.1420 | 1.4078 | 171 | 0.0198 | 3.8822 |
| 38 | 0.1364 | 6.2706 | 172 | 0.0197 | 5.1612 |
| 51 | 0.0864 | 5.9928 | 225 | 0.0168 | 0.8126 |
| 52 | 0.0839 | 0.6057 | 226 | 0.0168 | 4.3437 |

compared to a pure feedback strategy. The larger the PI, the larger the likelihood of observing a feedforward strategy in the HC. We investigate how the PI is affected by the relative strength of the target and disturbance signals and by the hypothesized imperfections in the feedforward, expressed in the HC model by parameters $T_I$ and $\tau_{p_t}$.

Performance is expressed by the root mean square (RMS) of the tracking error $e$, and the PI is expressed as a percentage:

$$\text{PI} = \frac{\text{RMS}(e_{\text{FB}}) - \text{RMS}(e_{\text{FB+FF}})}{\text{RMS}(e_{\text{FB}})} \times 100\% \qquad (7)$$

Subscript FB designates a pure feedback HC model ($K_{p_t} = 0$), and subscript FB + FF designates a model with an ideal feedforward contribution ($K_{p_t} = 1$). A PI of zero indicates no benefit of feedforward (equal performance with and without feedforward), a PI of 100% means that feedforward reduced the $\text{RMS}(e)$ to zero (perfect tracking), and negative PI values indicate a detrimental effect of feedforward on performance.

### A. Simulation properties

Simulations were performed with the models of Section III and parameter values of Table I, unless stated otherwise. The target and disturbance signals are identical to those in the human-in-the-loop experiment, see Fig. 6. The ramp and parabola target signals consist of one short (3.75 s) upward segment, five longer (7.5 s) alternately downward and upward segments, followed by a final short (3.75 s) upward segment.
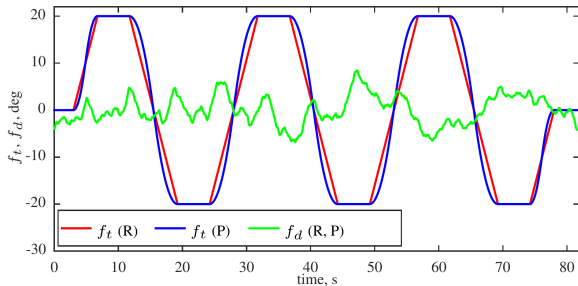


Fig. 6.   Target and disturbance signals. See Fig. 3 for individual ramp and parabola segments. For visibility, the disturbance signal is shown for $K_d = 3$.

The unpredictable sum-of-sines disturbance signal $f_d$ consists of twenty frequency components (Table II) generated by:

$$f_d(t) = K_d \sum_{i=1}^{20} A_{f_d}(i) \sin\left(n_{f_d}(i)\omega_m t + \phi_{f_d}(i)\right), \quad (8)$$

with $\omega_m = 2\pi/T_m$ and $T_m$ the measurement time equal to 81.92 s. The phases of the sinusoids were chosen such that the signal appeared random.

### B. Relative strength of target and disturbance signals

First, the magnitude of $f_d$ is varied by multiplication with gain $K_d$ to modulate the emphasis on either target-tracking or disturbance-rejection. In Fig. 6 $f_d$ is plotted for $K_d = 3$, but note that during the human-in-the-loop experiment $K_d$ was set to 1. To cover a wide range between pure target-tracking and pure disturbance-rejection tasks, we consider $0.1 < K_d < 100$.

Fig. 7(a) shows that, for all conditions, the PI is positive and it is largest for low values of $K_d$, indicating that feedforward improves target tracking performance. The PI is almost zero for high $K_d$, corresponding to a task with strong disturbances that can be rejected through feedback only. Here, target-tracking performance contributes little to task performance, and thus the PI due to feedforward is small.
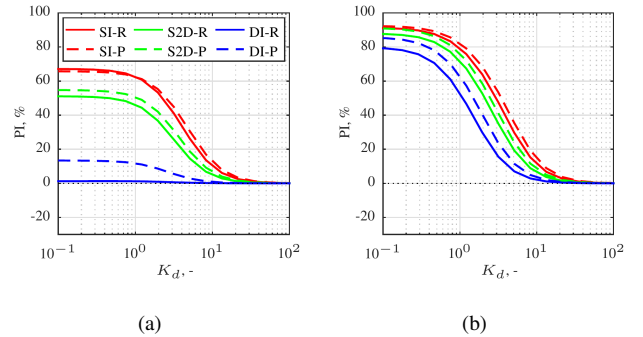


(a)          (b)

Fig. 7.   The performance advantage of the feedforward HC model for six different conditions, as a function of $K_d$ for different values of $T_I$ and $\tau_{p_t}$. (a) $T_I$ and $\tau_{p_t}$ as defined in Table I. (b) $T_I = 0.05$ s and $\tau_{p_t} = 0.05$ s.

Comparing across conditions, Fig. 7(a) shows that the PI is largest and always positive for both SI conditions, slightly smaller but still positive for both S2D conditions, and smallest for both DI conditions, for all values of $K_d$. For the DI-P condition a small PI is attainable through feedforward, but for the DI-R condition the PI is almost equal to zero. Here, feedforward improves performance minimally.

The minor PI in the DI-R condition is caused by 1) limitations and imperfections in the feedforward control strategy (modeled by $T_I$ and $\tau_{p_t}$) which cause $u_{p_t}$ to be considerably different from the optimal control input, and 2) the subsequent interaction between the simultaneously operating feedback and feedforward. The feedforward ideally generates a short, pulse-like control input that accelerates the system to the velocity of the ramp. The actual feedforward input is delayed by $\tau_{p_t}$ and is less 'pulse-like' due to the low-pass filter, resulting in

a large tracking error following the ramp onset. If $\tau_{p_e} \approx \tau_{p_t}$, the feedback will simultaneously respond to this error, causing the system to overshoot the target. Thus, performance does not improve by applying feedforward with a large $\tau_{p_t}$ and $T_I$.

For illustration, simulations were performed with $T_I = 0.05$ s and $\tau_{p_t} = 0.05$ s, see Fig. 7(b). These parameter values correspond to a hypothetically very skillful HC that is able to accurately predict the ramp onsets and give sharp, pulse-like control inputs of the correct magnitude and duration. The actual feedforward control input resembles the ideal input better and indeed the PI is much larger for small values of $K_d$ for *all* conditions, including the DI-R condition.

### C. Anticipating the Target Signal

A well-trained HC might *anticipate* the future course of the target and effectively have a *negative* time delay with respect to $f_t$. The PI was calculated as a function of $\tau_{p_t}$ to investigate the potential benefits of anticipatory inputs. Here, $T_I$ was set to 0.05 and 0.15 s (different from Table I) to illustrate the effect of $\tau_{p_t}$ and the interaction between $\tau_{p_t}$ and $T_I$.
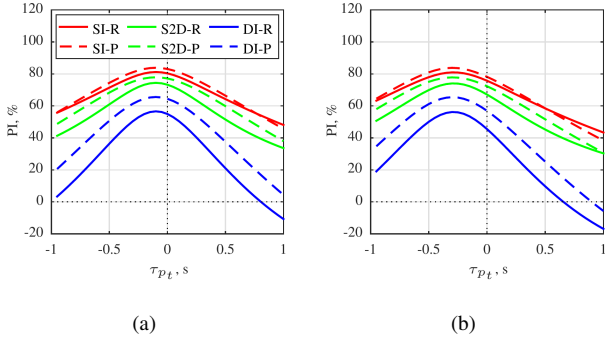


Fig. 8. The PI as a function of $\tau_{p_t}$, for $K_d = 1$ and all model parameters fixed. (a) $T_I = 0.05$ s. (b) $T_I = 0.15$ s.

Fig. 8 shows that $\tau_{p_t}$ has a large effect on the PI in all conditions for both values of $T_I$. Clearly, an optimal time delay $\tau_{p_t}^{\text{opt}}$ exists where the PI is largest, which is smaller than zero and depends on $T_I$. For $T_I = 0.05$ s, $\tau_{p_t}^{\text{opt}} \approx -0.1$ s; and for $T_I = 0.15$ s $\tau_{p_t}^{\text{opt}} \approx -0.30$ s. The low-pass filter smoothens $u_{p_t}$, but also increases lag. The anticipatory time delay compensates for this additional lag, such that $\tau_{p_t}^{\text{opt}}$ is more negative for larger $T_I$. In [14], $T_I$ values larger than 0.15 s were estimated from experimental data, so the HC has incentive to anticipate the target to improve performance. Note that [14] focused on the ramp onsets, and thus removed the ramp endings from the parameter estimation analysis after subjects reported they were able to anticipate these endings, explaining why [14] found positive feedforward time delays.

## V. EXPERIMENT

A human-in-the-loop experiment was conducted to validate the proposed HC models and to test the hypotheses derived from computer simulations with these models.

### A. Method

*1) Apparatus:* The tracking task, representing an aircraft pitch control task, was presented on a central visual display in a pursuit configuration, that explicitly shows the target $f_t$, perturbed system output $\theta$ and tracking error $e$ [see Fig. 2]. The ViewPixx Lite display, with an update rate of 120 Hz, has a (measured) time delay of 15 ms, was located 90 cm from the subject's eyes. The area used for the pursuit display was 800 by 800 pixels large. The display gain was 16 pixels per degree. No outside visuals and no motion cues were available.

Subjects used the fore/aft axis of an electrically-actuated sidestick to give their control inputs, $u$. The stick, with the application point of the subject's hand 9 cm above the rotation point, had no break-out force and a maximum deflection of $\pm 17$ deg. Its stiffness was set to 1.0 N/deg over the full deflection range, and its inertia to 0.01 kg $\cdot$ m$^2$; the damping coefficient was 0.2. The lateral stick axis was locked.

*2) Independent Variables:* Three different system dynamics, given in (1) through (3), and three different target signals (R, P and Z, see Section II-B) were varied in the experiment. Each subject performed each combination of system dynamics and target signal, resulting in a total of nine conditions.

*3) Subjects and Instructions:* Twelve subjects, eleven males and one female, aged 24-34 years (29 years avg.), were instructed to minimize the pitch tracking error $e$. The mean square of the error $e$ was displayed after each run.

*4) Procedure:* Subjects performed the nine conditions in three separate sessions. In each session, the system dynamics were constant and all three target signal variations were performed. The order of the sessions and the target signals were randomized by a Latin Square design.

The individual tracking runs lasted 90 seconds, of which the last 81.92 seconds were the measurement data, sampled at 100 Hz. Tracking performance was monitored by the experimenter: when performance had reached an asymptote, five repetitions were collected as the measurement data. The time traces of $e$, $u$ and $\theta$ were averaged over the five repetitions to reduce remnant, yielding one time trace for each subject for each condition. Note that averaging might blur distinctive features of feedforward, see [14]. Here, we insist on averaging over five runs to be consistent with the ARX method [18].

### B. Dependent Measures

*1) Nonparametric Measures:* Tracking performance was measured by the root mean square (RMS) of the error signal.

*2) Black-box ARX Identification:* The control behavior during the ramp and parabola conditions are identified by means of the black-box ARX identification method of [18]. It was developed to objectively identify *if* and *how* the HC utilizes a feedforward and/or feedback control strategy, without making any prior assumptions concerning the HC dynamics. The method fits and evaluates many ARX models in parallel and selects the best model based on the quality of the fit and the model complexity, measured by the number of free parameters. The generic structure of each ARX model is shown in Fig. 9 and is described by the discrete time difference equation of (9), with $k$ denoting the discrete time samples of 0.04 s (the
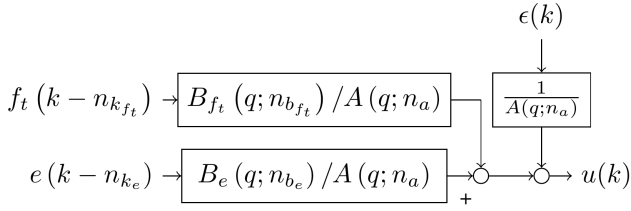
Fig. 9.   Generic ARX model structure.

data are resampled to 25 Hz prior to identification, to reduce estimation bias due to noise, and to reduce computation time).

$$A(q; n_a)u(k) = \begin{aligned} &B_{f_t}(q; n_{b_{f_t}})f_t(k - n_{k_{f_t}}) + \\ &B_e(q; n_{b_e})e(k - n_{k_e}) + \epsilon(k) \end{aligned} \quad (9)$$

In (9), $\epsilon$ is a white noise signal, $q$ is the delay operator and the polynomials $A$, $B_{f_t}$, and $B_e$ are defined in (10).

$$\begin{aligned} A(q; n_a) &= 1 + a_1 q^{-1} + \ldots + a_{n_a} q^{-n_a} \\ B_{f_t}(q; n_{b_{f_t}}) &= b_{f_t,1} + b_{f_t,2} q^{-1} + \ldots + b_{f_t,n_{b_{f_t}}} q^{\left(-n_{b_{f_t}}+1\right)} \\ B_e(q; n_{b_e}) &= b_{e,1} + b_{e,2} q^{-1} + \ldots + b_{e,n_{b_e}} q^{\left(-n_{b_e}+1\right)} \end{aligned} \quad (10)$$

Each ARX model is described by three model orders and one or two time delay parameters: the number of parameters in the $A$ polynomial $n_a$, the number of parameters in the $B_{f_t}$ polynomial $n_{b_{f_t}}$, the number of parameters in the $B_e$ polynomial $n_{b_e}$, the feedforward time delay $n_{k_{f_t}}$, and the feedback time delay $n_{k_e}$. Time delays are expressed in integer multiples of the sample time 0.04 s. The total number of free parameters $d$ is the sum of $n_a$, $n_{b_{f_t}}$ and $n_{b_e}$, and the number of time delay parameters. For a pure feedback model, $d$ is equal to $n_a + n_{b_e} + 1$; for a combined feedforward and feedback model $d = n_a + n_{b_{f_t}} + n_{b_e} + 2$. The ARX feedforward path requires at least 2 parameters to describe the inverse dynamics of a SI and the low-frequency range of the S2D dynamics, and at least 3 parameters to describe the inverse of a DI.

The ARX models are estimated from the first 40.96 s (1024 samples) of each set of data, and evaluated on the last 40.96 s. The model with the lowest "modified Bayesian Information Criterion" (mBIC) value [18], [21] is selected as 'best' model:

$$\text{mBIC} = \log V + c\frac{d \log N_d}{N_d}, \quad (11)$$

where $N_d$ equals the number of data samples used to calculate $V$, $c$ is the 'model complexity penalty parameter', and

$$V = \frac{1}{N_d} \sum_{k=N_d+1}^{2N_d} \left(u(k) - \hat{u}(k)\right)^2, \quad (12)$$

measures the quality of the fit, with $N_d = 1024$. In (12), $\hat{u}$ is the control signal calculated by the model through simulation. We set $c = 3$, based on a Monte Carlo analysis with a known model very similar to the expected HC dynamics, as described in detail in [18]. This particular value of $c$ will prevent 'false-positive' feedforward identification (i.e., a feedforward model selected from data generated by a pure feedback model).

The target signal $f_t$ was shifted 1 s backward in time (in similar fashion as in Section III) to allow for the identification of negative feedforward time delays. Table III shows the range of ARX model orders tested in full-factorial fashion. A total of 336,000 ARX models were identified and considered.

TABLE III
RANGE OF TESTED ARX MODEL ORDERS

| Order | $n_a$ | $n_{b_{f_t}}$ | $n_{b_e}$ | $n_{k_{f_t}}$ | Equiv. $\tau_{p_t}$ s | $n_{k_e}$ | Equiv. $\tau_{p_e}$ s |
|---|---|---|---|---|---|---|---|
| LB | 1 | 0 | 0 | 1 | -0.96 | 1 | 0.04 |
| UB | 7 | 7 | 7 | 50 | 1.0 | 15 | 0.6 |

*3) Parametric Model Parameter Estimation:* We will fit six parametric models, based on the ARX results and literature, by means of the time domain estimation method of [19], to obtain insight in the best model structure and the adaptation of the HC. The quality of the obtained models is compared through the Variance Accounted For (VAF):

$$\text{VAF} = \left(1 - \frac{\sum_{k=0}^{N-1} |u(k) - \hat{u}(k)|^2}{\sum_{k=0}^{N-1} u(k)^2}\right) \times 100\%, \quad (13)$$

with $\hat{u}$ the modeled, and $u$ the measured control signal.

*C. Hypotheses*

Simulations showed that feedforward improves performance for all conditions, but only in specific circumstances for the DI-R condition. Ref. [14] found evidence for feedforward for all system dynamics considered here with a ramp target, but results were less consistent across subjects for the DI. Therefore, we expect to identify a feedforward operation for all subjects in all conditions, except in the DI-R condition. Here we expect considerable variability between subjects. (H.I)

The required feedforward control inputs $u_{p_t}$ for the parabola target appear more complex than for the ramp target. That is, $u_{p_t}$ has a triangular waveform for SI-P and S2D-P, and consists of two plateaus of opposite sign for DI-P, whereas it is one simple plateau for SI-R and S2D-R, and mostly zero for DI-R, see Fig. 5. The parabola target requires the HC to match both velocity and acceleration, which is possibly more difficult than matching the ramp velocity. We expect the feedforward to be weaker (lower $K_{p_t}$) and more 'cautious' (reflected by a higher $T_I$) for the parabola than for the ramp.

We expect to find evidence for anticipatory feedforward control, indicated by negative $\tau_{p_t}$, but possibly only for very skilled subjects and not in all conditions. (H.III)

VI. EXPERIMENT RESULTS

*A. Measured Time Traces*

Representative time traces of the measured control signal $u$, error $e$, and output $\theta$ during a single ramp and parabola segment are plotted in Fig. 10, for all R and P conditions.

Fig. 10(a) shows the control signal $u$ measured during ramp segments for all three system dynamics. The measured control signal is similar to the feedforward signal generated by the model, see Fig. 5(a), but also contains the effect of
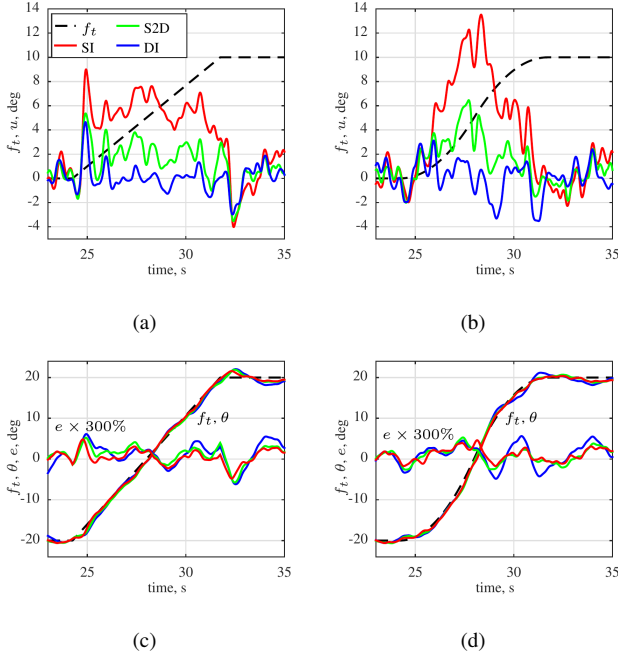
Fig. 10. Representative time traces (subject 1). (a) and (b) Control signal $u$ for ramp and parabola conditions, respectively. Target $f_t$ scaled by 0.25 and shifted up. (c) and (d) Target $f_t$, system output $\theta$ and tracking error $e$ (scaled by a factor 3) for ramp and parabola conditions, respectively.

the disturbances. For SI-R $u$ is similar to a plateau, for S2D-R it resembles a pulse followed by a plateau, and for DI-R two pulses around the ramp onset and endings can be distinguished. A similar resemblance between $u$ measured during the parabola segments and the models' feedforward signal is observed, see Fig. 10(b) and Fig. 5(b). For SI-P and S2D-P $u$ resembles a triangle, and for DI-P $u$ resembles two small plateaus of opposite sign. Note that the resemblance between the ideal and measured control signals does not provide evidence regarding the utilized control strategy.

Figs. 10(c) and 10(d) show that subjects could track the target signals adequately, with errors smaller than $\pm 5$ deg. Spikes in the error signal around the onset of the parabolas were smaller than for the ramps.

### B. Tracking performance

Fig. 11 shows the RMS error $e$, for each condition, averaged over all subjects. Error bars indicate the 95% confidence intervals corrected for between-subject variability. For all targets, performance was best for SI dynamics, then S2D dynamics, and worst for DI dynamics. For all dynamics, performance was best for the zero target signal, where subjects could focus entirely on the rejection of the disturbances, then the parabola, and worst for the ramp. Performance was better for the parabola than for the ramp, because the error increases slower just following the sudden onsets of the parabola segments than following the ramp onsets, see Fig. 10(c) and Fig. 10(d) at 24 and 32 s. These results contradict hypothesis H.II; apparently, parabolas were not more difficult to track than ramps.

### C. Black-Box ARX Identification Results

*1) Results as a function of c:* Fig. 12(a) shows how the quality of the selected ARX models, measured by the VAF, depends on the value of $c$, averaged over all subjects. Data are presented on a logarithmic scale; the value of $c$ ($= 3$), for which all subsequent results are shown, is marked by a vertical dashed line. As expected, model quality is high for small $c$ and decreases for larger $c$. The VAF first decreases slowly, but then, at a specific value of $c$, it decreases rapidly. For the SI conditions this 'knee point' is seen at $c \approx 80$ and 150 (ramp and parabola, respectively) and for both S2D conditions at 40. The curves for DI-R and DI-P are more separated and the knee points at $c \approx 70$ for DI-R and at 30 for DI-P are less abrupt, suggesting a larger between-subject variability.

Fig. 12(b) shows how the number of parameters (model complexity) in the feedforward path $n_{b_{f_t}}$ depends on $c$. Note that the ARX model for each individual subject has an integer number of parameters; fractional results are caused by averaging over 12 subjects. For the SI and S2D conditions, a 'knee point' is seen at exactly the same values of $c$ for which the quality of the model decreased rapidly. This indicates that the feedforward path indeed contributes heavily to the model.

A strong correlation between the model quality and model complexity metrics is seen for the DI-P condition, but they do not show a clear 'knee point'. That is, both the number of feedforward parameters and the model quality decrease for larger $c$, but not very abruptly. The results are averaged over subjects and the lack of a knee point could indicate larger differences between subjects' feedforward usage than in the SI and S2D conditions. We conclude that for the DI-P condition the feedforward path is an essential model component.

Finally, for the DI-R condition there is little relation between Fig. 12(a) and Fig. 12(b). Although the feedforward path on average contains less than 1 parameter for $c = 6$ the VAF is still well above 80%: only a few percentage points lower than for $c = 1$. It seems that the feedforward path is not an essential part of the HC model for DI-R and could be left out.

Based on the results obtained as a function of $c$, we see no reason to change our choice to use $c = 3$, which was based on Monte Carlo simulations [18]. For $c = 3$, the VAF of the selected model is almost as high as for much smaller values of $c$, but the models contain fewer parameters, suggesting that these additional parameters are not needed to describe HC control dynamics.

The histogram in Fig. 12(c) shows the number of subjects for which a model with a particular number of feedforward parameters was selected, to assess the consistency of the selected models across subjects for $c = 3$. It shows that in all SI and S2D conditions, a model with at least 2 feedforward parameters was selected. For the DI-P condition the selected models are consistent as well, with ten out of twelve subjects for which $n_{b_{f_t}} = 3$ and the remaining $n_{b_{f_t}} = 0$. In the DI-R condition a large variation is seen across subjects, illustrating that the feedforward contribution is small and inconsistent.

*2) Single integrator dynamics (SI):* Figs. 13(a) and (b) show the feedforward ($\hat{Y}_{p_t}$) and feedback ($\hat{Y}_{p_e}$) frequency responses of the selected ARX models ($c = 3$) for the SI-R condition of all subjects. The range for which the results
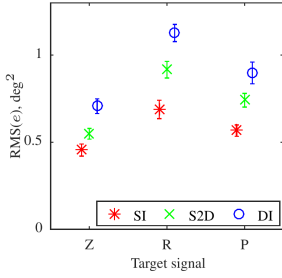
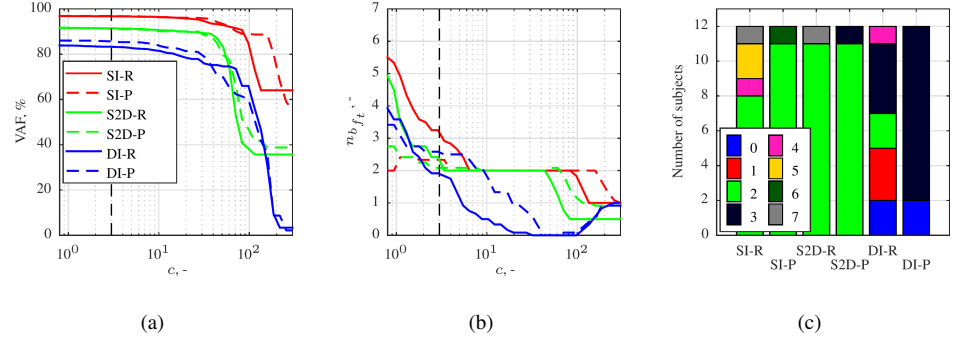Fig. 11. The RMS of the tracking error for all conditions.



Fig. 12. Model selection results. (a) The VAF of the selected ARX models as a function of $c$, averaged over all subjects. (b) The number of parameters in the feedforward path $n_{b_{f_t}}$ of the selected ARX models as a function of $c$, averaged over all subjects. (c) Histogram of $n_{b_{f_t}}$ of the selected ARX models counted by subject, for $c = 3$.

are valid is indicated with two dashed vertical lines, marking the lowest and highest frequency component in the disturbance signal. Outside this frequency range, the HC dynamics were not simultaneously exited by two uncorrelated forcing functions, and therefore the estimates are not strictly valid.

Fig. 13(a) shows that for *all* subjects a feedforward response was identified that approximates inverse SI dynamics. That is, the magnitude plot has a slope equal to a differentiator and the phase is close to +90 deg at frequencies lower than 1 rad/s for most subjects. Between 1 and approximately 8 rad/s, the magnitude of the feedforward response levels off in similar fashion to a low-pass filter with a corner frequency between 1 and 4 rad/s. At even higher frequencies, most responses show a peak similar to the NMS peak in the feedback path. Furthermore, the phase response suggests that a considerable time delay was present in the feedforward for most subjects. The two subjects for which the phase becomes exponentially positive correspond to selected models with a negative time-delay, evidence for their anticipation of the target signal.

Fig. 13(b) shows the identified feedback response of all subjects. The structure of the feedback responses are as expected for SI dynamics based on McRuer's Extended Crossover Model [11]: they resemble a gain at lower frequencies and have a neuromuscular peak around 10 rad/s.

Figs. 13(c) and (d) show the frequency responses of the selected ARX models for the SI-P condition. Results are very similar to the SI-R condition. The feedforward response resembles inverse system dynamics for all subjects at low to medium frequencies. The corner frequency of the apparent low-pass filter is more consistent across subjects and at a lower frequency (around 1 rad/s). The exponentially positive phase responses indicate that all but one subject *anticipated* for the target signal, suggesting a negative feedforward time delay.

Feedback responses are very similar to those identified for the SI-R condition, but are less consistent across subjects.

*3) Second-order system (S2D):* Figs. 14(a) and (b) show the feedforward and feedback frequency responses of the selected ARX models for the S2D-R condition. For *all* subjects a feedforward response was identified that follows the inverse system dynamics closely below 1 rad/s. It resembles a differentiator up to 10 rad/s, where a NMS peak is seen. A considerable time delay is present for all but one subject. The feedback

response [see Fig. 14(b)] resembles the Extended Crossover Model: a gain at lower frequencies, a lead around crossover and a neuromuscular peak around 10 rad/s. The phase response provides evidence for a considerable time delay.

The primary difference in the feedforward responses between S2D-R and S2D-P [see Fig. 14(c)] is the phase: for S2D-P the subjects anticipate for the target signal. The feedback responses of S2D-P [see Fig. 14(d)] are very similar to S2D-R and resemble the Extended Crossover Model.

*4) Double integrator dynamics (DI):* Figs. 15(a) and (b) show the frequency responses of the selected ARX models for the DI-R condition. The five subjects for which $0 < n_{b_{f_t}} < 3$ are plotted in a different style, for easy comparison with the theoretically ideal $1/Y_c$ feedforward. For five other subjects a model for which $n_{b_{f_t}} \geq 3$ was selected: these models follow the inverse system dynamics, albeit with a low gain ($\approx 0.2$), suggesting that these subjects utilized feedforward. The selected models of the remaining two subjects had $n_{b_{f_t}} = 0$, as it is not clear whether they utilized feedforward. It is possible that the subjects used a feedforward for certain ramps, but not for all, resulting in an ambiguous model selection. The feedback dynamics are similar to the Extended Crossover Model: a low frequency gain and a lead around crossover.

Figs. 15(c) and (d) show the frequency responses of the selected ARX models for the DI-P condition. The feedforward responses of ten subjects approximate $1/Y_c$, but with a smaller magnitude than the ideal. For these subjects, $n_{b_{f_t}} = 3$, which is needed to invert the double integrator. A low-pass filter is not present, possibly because its effect is too small and the NMS affects the feedforward control signal in a similar way. The phase shows strong variation between subjects, likely due to high remnant levels, common for DI dynamics, and the small contribution of the feedforward. The feedback responses are again very similar to the Extended Crossover Model.

### D. Time Domain Parameter Estimation Results

Now that the black-box ARX method identified a feedforward response approximating inverse system dynamics consistently across subjects for all SI and S2D conditions and the DI-P condition, it is considered appropriate to fit parametric HC models to gain further insight in the precise feedforward dynamics. The ARX method did not reveal the order of the
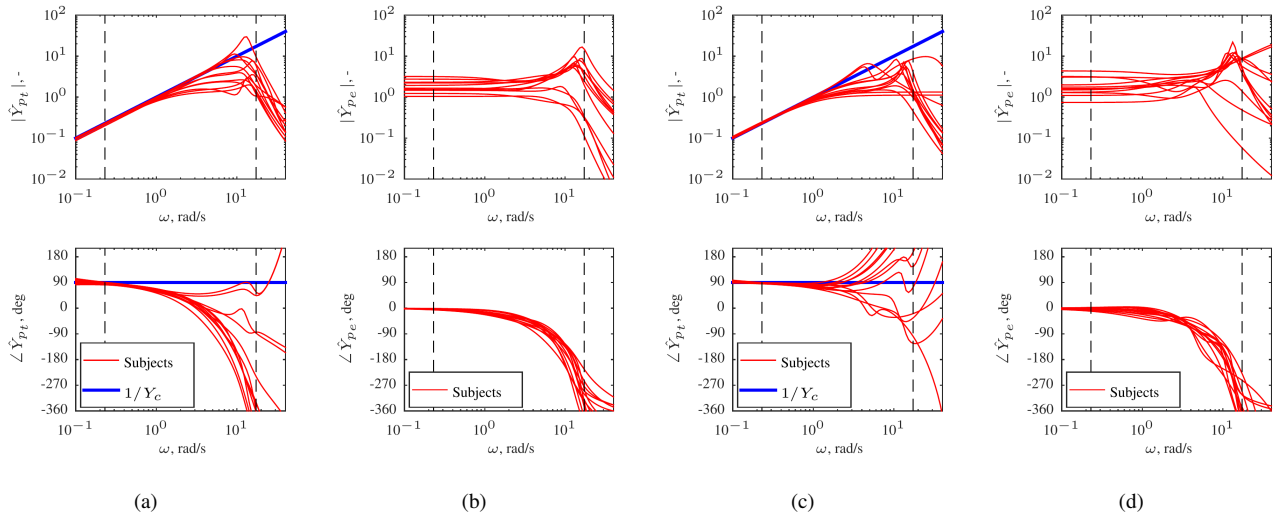
Fig. 13. The frequency response of the selected ARX models for $c = 3$ for all subjects. (a) SI-R, $\hat{Y}_{p_t}$. (b) SI-R, $\hat{Y}_{p_e}$. (c) SI-P, $\hat{Y}_{p_t}$. (d) SI-P, $\hat{Y}_{p_e}$.
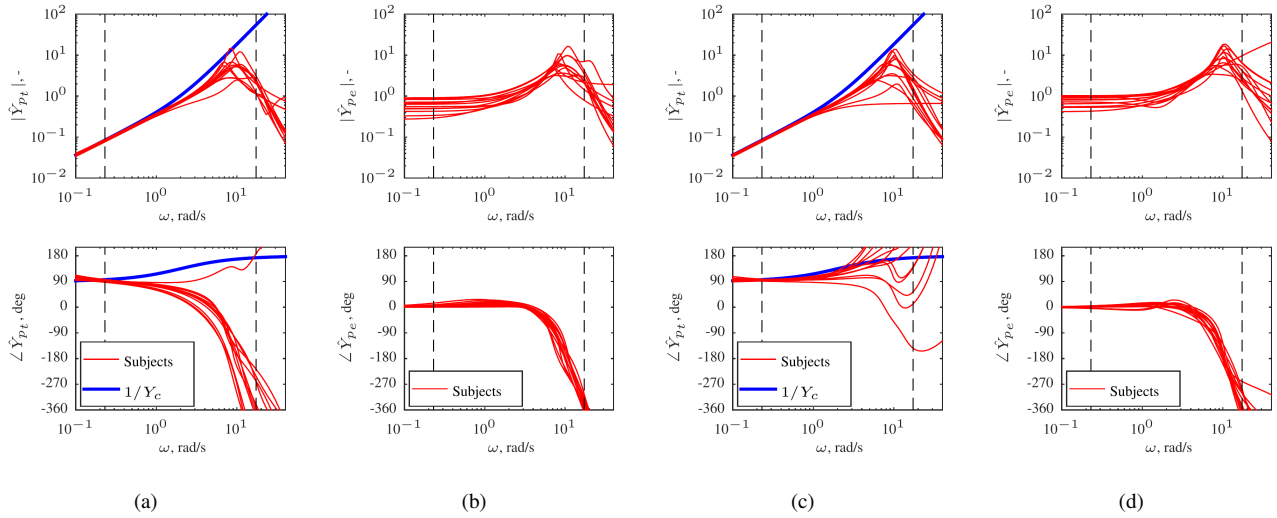


Fig. 14. The identified ARX models for all subjects, condition S2D-R. (a) S2D-R, $\hat{Y}_{p_t}$. (b) S2D-R, $\hat{Y}_{p_e}$. (c) S2D-P, $\hat{Y}_{p_t}$. (d) S2D-P, $\hat{Y}_{p_e}$.



Fig. 15. The identified ARX models for all subjects for DI conditions. For DI-R, an ARX model without feedforward contribution was selected for 3 out of 12 subjects, for DI-P for 2 out of 12 subjects. (a) DI-R, $\hat{Y}_{p_t}$. Note the deviating range of the ordinate axis from the other presented Bode plots. (b) DI-R, $\hat{Y}_{p_e}$. (c) DI-P, $\hat{Y}_{p_t}$. (d) DI-P, $\hat{Y}_{p_e}$.

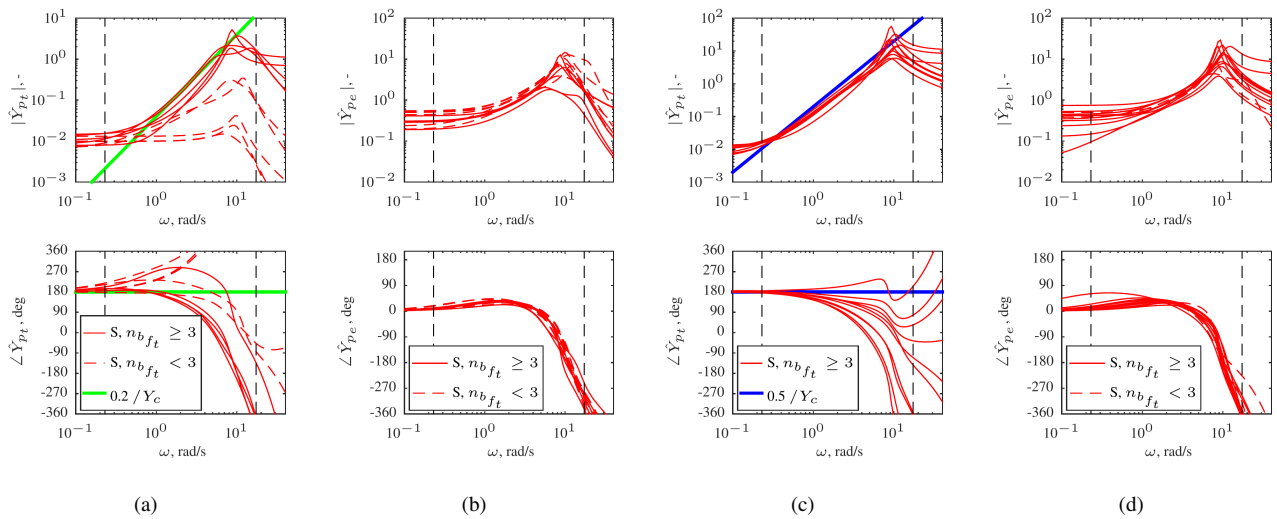low-pass filter and even suggested that it is not required in the DI conditions. Also, all feedforward responses included NMS dynamics, but this is possibly due to the common denominator of the feedforward and feedback paths in the ARX models: either both paths have NMS dynamics, or none.

We attempt to reveal the best feedforward model by fitting six candidate models: the different models contain either no low-pass filter (nLPF), a first-order low-pass filter (LPF1), or a second-order low-pass filter (LPF2), and the NMS acts either on the feedback path only (nNMS), or on the feedforward and feedback path simultaneously (NMS). For example, the model with a first-order low-pass filter and the NMS acting on both paths simultaneously is designated NMS-LPF1.

Fig. 16 shows the VAF of the six candidate models for all conditions. VAF values are large for all models and all conditions and differences between models are small. Differences in VAF are largest between models without a low-pass filter and models including a filter, with the LPF2 models slightly better than LPF1 models for all conditions, but not statistically significant. A choice for a model with a second order low-pass filter seems justified based on these results, for its consistently higher VAF for *all* conditions. Comparing nNMS-LPF2 to NMS-LPF2, no significant differences are seen, most likely because the second-order filter removes virtually all high frequency content from $f_t$ and thus the NMS does not affect the feedforward control signal. The choice for the 'best' model structure remains ambiguous; here we choose the nNMS-LPF2 model for further analysis, also to be consistent with [14].

*1) SI and S2D Conditions:* Fig. 17 shows the mean and 95% confidence intervals of the estimated model parameter values for the nNMS-LPF2 model, for all subjects and all conditions. The estimates are generally consistent across subjects, with the ARX analysis and with literature [14], [17]. For the Z conditions, the fit model was identical to the nNMS-LPF2 model, except that the feedforward path was removed. Hence, only estimates for the compensatory and neuromuscular elements are shown for these conditions.

We decided not to do a statistical analysis concerning the significance of observed differences and trends, because 1) different models were fit to the Z condition (feedback

only) and the R and P conditions (feedforward/feedback), 2) different models were fit to the SI conditions and the S2D and DI conditions (additional lead term), and 3) the ARX analysis showed that HC behavior in the DI-R condition requires a different HC model than the one used in this analysis.

The feedforward gain $K_{p_t}$ is slightly lower than 1 for all conditions except SI-P, where the estimated value is slightly above 1. In previous studies involving ramps, $K_{p_t}$ was indeed found to be lower than 1, believed to reflect a strategy to prevent overshoot at the end of a ramp segment. Overshoot is less likely with the parabola, because it has a lower velocity towards the end, explaining slightly higher values for $K_{p_t}$ here.

The feedforward time delay $\tau_{p_t}$ depends strongly on the target signal: it is close to zero for SI-R and S2D-R, but negative for SI-P and S2D-P, indicating anticipatory control inputs. In [14], the estimated values for $\tau_{p_t}$ were larger than zero, most likely because all ramp endings were removed from the analysis after subjects reported that these were easier to anticipate than ramp onsets. Here, the individual ramp segments were also shorter and more tightly spaced, making it easier to predict the ramp onsets and endings.

Estimated values for $T_I$ are similar to [14] despite the previously described differences in the analysis. For S2D-R, the mean and confidence intervals do not represent the distribution well, as one outlier result is situated at $T_I = 0.95$ s. $T_I$ is smaller for ramp than for parabola targets; reflecting a quicker response with more high-frequency content. Because subjects can anticipate the parabola better than the ramp, there is possibly less incentive to give quick, aggressive control inputs; a gentle, well-timed input is sufficient.

The feedback gain $K_{p_e}$ and lead time constant $T_L$ depend on the system dynamics only, not on the target. They are similar to values found in literature [14], [17]. For the SI, $\tau_{p_e}$ was found to be higher for the parabola than the ramp. The maximum velocity of the parabola target is larger than the ramp velocity; larger time delays were also found for faster ramps in [17]. Finally, $\omega_{nms}$ and $\zeta_{nms}$ depend only on the system dynamics.

*2) DI Conditions:* Individual subject results are plotted next to the mean and confidence intervals in Fig. 17, because of the non-uniform ARX model selection in DI conditions [see Fig. 12(c)]. Three parameters are necessary to describe inverse dynamics of a DI, therefore subjects for which the selected model had fewer parameters are marked differently.

For the DI-P condition, $K_{p_t}$ estimates are consistent with the ARX results: the two subjects for which a pure feedback model was selected have a considerably smaller feedforward gain than the other subjects. This is the first reliable feedforward identification for the DI: it was identified through a black-box ARX method first, followed by a parameter estimation analysis that provides consistent results.

For the DI-R condition, however, there is no apparent correlation between $K_{p_t}$ and the ARX results. The feedforward contribution is small and short, and concentrated around the ramp discontinuities where human remnant is large, resulting in a large variability in the model selection. To obtain more insight in the DI-R condition, other analyses are necessary.

The low-pass filter time constant $T_I$ is larger for the DI-P than the SI and S2D conditions, and $\tau_{p_t}$ is estimated
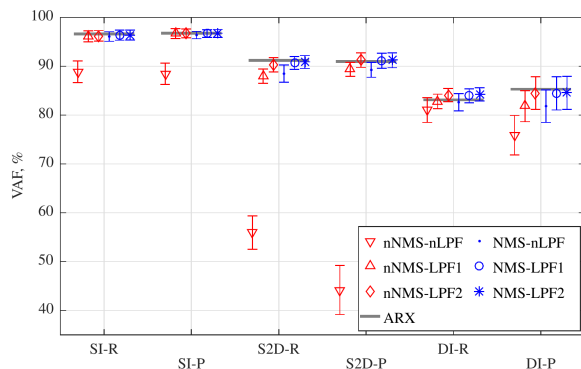


Fig. 16. The VAF of all six models for all ramp and parabola conditions averaged over all subjects, error bars show 95% confidence intervals corrected for between-subject variability.
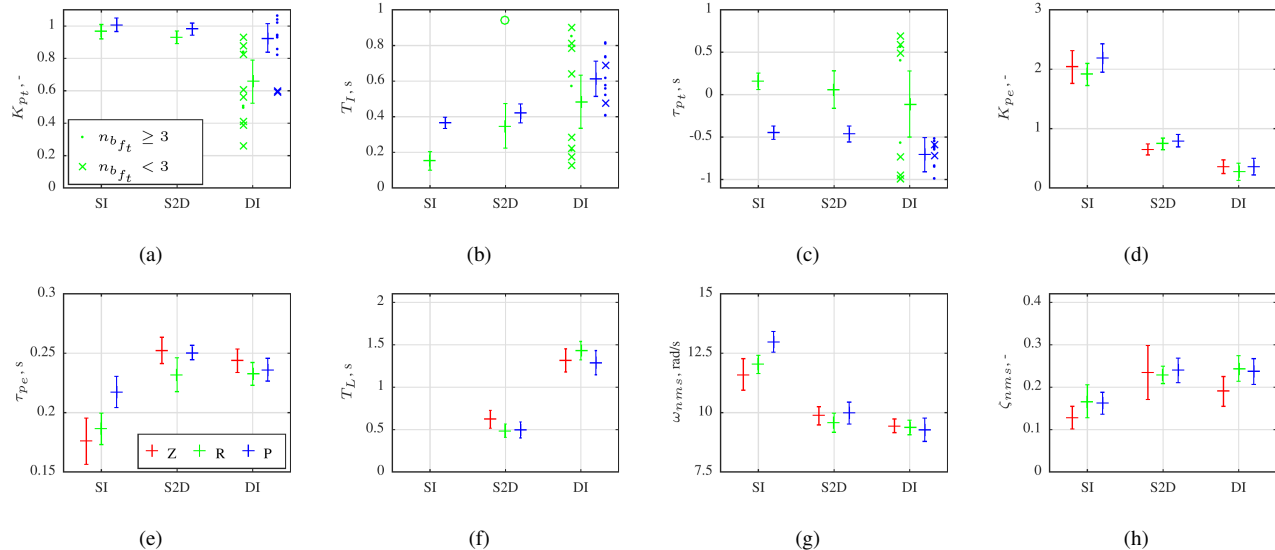
Fig. 17. Model fit parameter values averaged over all subjects, error bars show 95% confidence intervals corrected for between-subject variability.

strongly negative indicating anticipatory control inputs. These parameter values reflect a 'cautious' feedforward response: the inputs are smaller than ideal ($K_{p_t} \approx 0.9$), low-frequency, and anticipatory to prevent overshoot. Furthermore, the feedback estimates are consistent with the DI-Z condition and literature.

### E. Anticipatory Feedforward Control Inputs

The previous analyses suggest that the feedforward response is anticipatory in all parabola conditions. Evidence of anticipatory feedforward control is also found in recorded time traces. Fig. 18 compares the 'ideal' feedforward control signal $u_{p_t}^{\text{ideal}}(t) = f_t(t)/Y_c(s)$, to the measured control signal $u$ minus an estimate of the feedback contribution $\hat{u}_{p_e}(t) = e(t) \cdot Y_{p_e}(s) \cdot Y_{nms}(s)$, which is an estimate of $u_{p_t}$ without assuming a specific model for $Y_{p_t}$. Furthermore, $\hat{u}_{p_t}$ as provided by the NMS-LPF2 parametric model is shown.
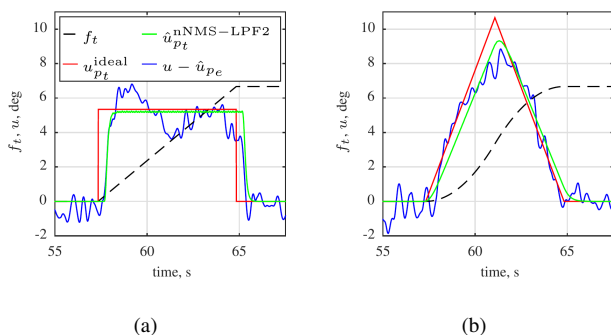


Fig. 18. Feedforward control signals for (a) SI-R and (b) SI-P.

For SI-R, Fig. 18(a), $u - \hat{u}_{p_e}$ is delayed with respect to $u_{p_t}^{\text{ideal}}$ following the target discontinuities (onset and endings of the ramp segment), while during the ramp segment it oscillates around the ideal feedforward input. The estimated feedforward control signal $\hat{u}_{p_t}^{\text{NMS}-\text{LPF2}}$ is also delayed (such that $\tau_{p_t} > 0$ s), and of slightly smaller magnitude than the ideal (such that $K_{p_t} < 1$), suggesting no anticipatory behavior.

For SI-P, Fig. 18(b), $u - \hat{u}_{p_e}$ is also delayed after the onset of the parabola segment, but is mostly 'synchronized' with or even leads $u_{p_t}^{\text{ideal}}$ *during* the remainder of the parabola segment. The sharp peak in $u_{p_t}^{\text{ideal}}$ around 60 s is absent from $u - \hat{u}_{p_e}$, demonstrating that subjects indeed provide a feedforward control input with a limited bandwidth ($T_I > 0$). Furthermore, it seems that at 59 s the feedforward control input $u - \hat{u}_{p_e}$ is reduced, in anticipation of the reversal in the target acceleration at 61 s, see also Fig. 3(b).

## VII. DISCUSSION

The ARX method provided strong evidence for an inverse system dynamics feedforward response on the target, confirming hypothesis H.I. It is the first identification of feedforward from experimental data using a black-box method that explicitly considers model complexity to prevent false-positive feedforward identification [18]. It is also the first feedforward identification for the difficult-to-control DI dynamics.

For the DI-R condition, the feedforward model has a good quality of fit ($>80\%$), but the feedforward parameter estimates are not consistent between subjects. The performance improvement analysis showed that feedforward is useful here only if the feedforward is fast and timed appropriately (anticipatory). Subjects likely attempt to give an anticipatory input at every ramp discontinuity, but succeed only for a few, depending on how well these can be predicted (e.g., by counting). The analysis method assumes behavior to be stationary over 81.92 s and is therefore not suited for the DI-R condition. This condition is not considered in the remainder of this discussion.

We expected that using a feedforward control operation would be more difficult for the parabola target signal (H.II), but no evidence was found to support this hypothesis. Contrary to our expectations, a slightly *stronger* feedforward response was found (larger $K_{p_t}$) for parabola conditions. Small differences in the low-pass filter settings were found for the SI only (larger $T_I$ for SI-P than SI-R), but these were not large enough to argue that a feedforward operation was more difficult.

Anticipatory feedforward control was identified in all conditions for one or more subjects, but mainly in parabola conditions, confirming hypothesis H.III. Possibly, the differences in the feedforward time delay between ramp and parabola conditions are caused by a complex interaction between non-linear HC behavior and the used (linear) identification methods. Two types of delay could have been present in the feedforward response of the HC: 1) a discrete reaction time in detecting the ramp or parabola onsets, and 2) a continuous delay *during* the ramp and parabola segments. Then, we observe that $\tau_{p_t}$ can be estimated only during time instances where $u_{p_t}$ is varying in time. For all ramp conditions, $u_{p_t}$ is time-varying around the discontinuities only, but otherwise constant. Hence, the analysis methods will identify the time delay just following the discontinuities, corresponding with the reaction time of approximately 200 ms [22]. For all parabola conditions, however, $u_{p_t}$ is time-varying throughout the entire parabola segment. Thus, $\tau_{p_t}$ is estimated close to the continuous time delay, which is negative for all but one subject.

In this experiment, the feedforward control behavior could have consisted of learned pre-cognitive motor commands. First, the HC cannot accurately perceive object acceleration [23], which would be required for visually guided pursuit control in the DI-P condition. Second, the anticipatory feedforward time delay suggests that the HC gives control commands *before* the target can be perceived visually. The pre-cognitive motor commands are triggered by the recognition of a ramp or parabola onset, after which they are executed in open-loop fashion. The actual control strategy is possibly considerably different from the one in the model used to analyze the results.

The identification method of [18] was developed to objectively identify HC dynamics from tasks involving realistic targets that possibly invoke feedforward control behavior. The model selection criterion is tuned through the model complexity penalty parameter $c$ based on the number of 'false-positive' or 'false-negative' results found in Monte Carlo simulations. The model complexity penalty parameter also provides an intuitive means to investigate the relation between model quality and complexity *post-hoc*. The complexity of the selected models does not change for a wide range of $c$ values, which is strong evidence for the feedforward model and warrants further analysis with the parameter estimation method. The identification method should not replace, but *complement* parameter estimation analyses in future studies.

We used simulations with HC models to investigate the performance improvement with feedforward and used this as a predictor for feedforward behavior. This approach has limited applicability, because the actual control strategy is different from the HC model; thus, the model needs further improvements. An important, but poorly understood aspect of feedforward behavior that needs to be addressed in future work is the *predictability* of the target signal [15], [24].

Finally, in this paper we studied the HC in control of stable, linear, vehicle-like dynamics. Establishing a theory that allows us to *predict* the systematic adaptation of the HC to these everyday dynamics would allow us to significantly improve our control interfaces. In rare situations, the HC might be (perhaps temporarily) confronted with unstable or nonlinear dynamics, for instance because of a system failure. Such unstable dynamics are likely similar to the S2D dynamics, but with an unstable pole ($\omega_b < 0$ rad/s) [11]. For such dynamics, it can be shown (through simulations equivalent to those presented in this paper) that an HC model with an inverse dynamics feedforward path results in stable tracking of a target signal. Furthermore, the potential performance improvement of feedforward is of the same order of magnitude as for the stable S2D dynamics. These simulations, however consider only the HC in steady-state, with fixed controlled element dynamics. Studying the HC response and adaptation to (sudden) changes in system dynamics, like from stable to unstable dynamics, would require a fundamentally different approach, and reaches beyond the state-of-the-art in cybernetics tools and methods [25]; it is one of the main avenues of future research.

## VIII. Conclusions

This paper studied the effects of target signal waveform shape and system dynamics on human feedforward control behavior in tracking tasks with predictable target signals and an unpredictable disturbance signal. Two target waveform shapes were evaluated, consisting of constant velocity ramp segments or constant acceleration parabola segments. Three vehicle-like system dynamics were investigated: a single integrator, a second-order system, and a double integrator. From a human-in-the-loop tracking experiment we conclude that: 1) a combined feedforward/feedback control strategy, modeled accurately by a quasi-linear model, was identified for all dynamics with the parabola target, and for the single integrator and second-order system with the ramp target; 2) evidence of non-stationary control behavior was found for the double integrator and ramp task; 3) the HC is able to anticipate the future course of the parabola target signal given extensive practice, reflected by *negative* feedforward time delay estimates; and 4) the feedforward model parameters are influenced by the target waveform shape. Model predictions of possible performance improvement show partial agreement with these results, notably the used model does not include the influence of target shape on feedforward parameters, a nonlinear effect that was apparent in the identified parameters.

## References

[1] J. Rasmussen, "Skills, Rules, and Knowledge; Signals, Signs, and Symbols, and Other Distinctions in Human Performance Models," *IEEE Trans. on Systems, Man, and Cybernetics*, vol. 13, no. 3, pp. 257–266, 1983.

[2] M. Mulder, D. A. Abbink, M. M. van Paassen, and M. Mulder, "Design of a haptic gas pedal for active car-following support," *IEEE Trans. on Intelligent Transportation Systems*, vol. 12, no. 1, pp. 268–279, 2011.

[3] D. A. Abbink, M. Mulder, F. C. T. van der Helm, M. Mulder, and E. R. Boer, "Measuring neuromuscular control dynamics during car following with continuous haptic feedback," *IEEE Trans. on Systems, Man, and Cybernetics – Part B: Cybernetics*, vol. 41, no. 5, pp. 1239–1249, 2011.

[4] D. A. Abbink and M. Mulder, "Neuromuscular Analysis as a Guideline in designing Shared Control," in *Advances in Haptics*. InTech, 2010, pp. 499–416.

[5] D. T. McRuer and H. R. Jex, "A Review of Quasi-Linear Pilot Models," *IEEE Trans. on Human Factors in Electronics*, vol. 8, no. 3, pp. 231–249, 1967.

[6] K. van der El, D. M. Pool, H. J. Damveld, M. M. van Paassen, and M. Mulder, "An Empirical Human Controller Model for Preview Tracking Tasks," *IEEE Trans. on Cybernetics*, vol. 46, no. 11, pp. 2609–2621, 2016.

[7] E. S. Krendel and D. T. McRuer, "A Servomechanics Approach to Skill Development," *J. of the Franklin Inst.*, vol. 269, no. 1, pp. 24–42, 1960.

[8] R. W. Pew, J. C. Duffendack, and L. K. Fensch, "Sine-Wave Tracking Revisited," *IEEE Trans. on Human Factors in Electronics*, vol. 8, no. 2, pp. 130–134, 1967.

[9] T. Yamashita, "Effects of Sine Wave Combinations on the Development of Precognitive Mode in Pursuit Tracking," *J. of Experimental Psychology*, vol. 42A, no. 4, pp. 791–810, 1990.

[10] R. J. Wasicko, D. T. McRuer, and R. E. Magdaleno, "Human Pilot Dynamic Response in Single-loop Systems with Compensatory and Pursuit Displays," Air Force Flight Dynamics Laboratory, Tech. Rep. AFFDL-TR-66-137, Dec. 1966.

[11] D. T. McRuer, D. Graham, E. S. Krendel, and W. Reisener Jr., "Human Pilot Dynamics in Compensatory Systems, Theory Models and Experiments with Controlled Element and Forcing Function Variations," Air Force Flight Dynamics Laboratory, Tech. Rep. AFFDL-TR-65-15, 1965.

[12] D. M. Pool, P. M. T. Zaal, H. J. Damveld, M. M. van Paassen, J. C. van der Vaart, and M. Mulder, "Modeling Wide-Frequency-Range Pilot Equalization for Control of Aircraft Pitch Dynamics," *J. of Guidance, Control, and Dynamics*, vol. 34, no. 5, pp. 1529–1542, 2011.

[13] G. C. Beerens, H. J. Damveld, M. Mulder, M. M. van Paassen, and J. C. van der Vaart, "Investigation into Crossover Regression in Compensatory Manual Tracking Tasks," *J. of Guidance, Control, and Dynamics*, vol. 32, no. 5, pp. 1429–1445, 2009.

[14] V. A. Laurense, D. M. Pool, H. J. Damveld, M. M. van Paassen, and M. Mulder, "Effects of Controlled Element Dynamics on Human Feedforward Behavior in Ramp-Tracking Tasks," *IEEE Trans. on Cybernetics*, vol. 45, no. 2, pp. 253–265, 2015.

[15] R. E. Magdaleno, H. R. Jex, and W. A. Johnson, "Tracking Quasi-Predictable Displays Subjective Predictability Gradations, Pilot Models for Periodic and Narrowband Inputs," in *Fifth Annual NASA-University Conference on Manual Control*, 1969, pp. 391–428.

[16] D. M. Pool, M. M. van Paassen, and M. Mulder, "Modeling Human Dynamics in Combined Ramp-Following and Disturbance-Rejection Tasks," in *Proc. of the AIAA Guidance, Navigation, and Control Conf.*, no. AIAA-2010-7914, 2010.

[17] F. M. Drop, D. M. Pool, H. J. Damveld, M. M. van Paassen, and M. Mulder, "Identification of the Feedforward Component in Manual Control With Predictable Target Signals," *IEEE Trans. on Cybernetics*, vol. 43, no. 6, pp. 1936–1949, 2013.

[18] F. M. Drop, D. M. Pool, M. M. van Paassen, M. Mulder, and H. H. Bülthoff, "Objective Model Selection for Identifying the Human Feedforward Response in Manual Control," *IEEE Trans. on Cybernetics*, vol. PP, no. 99, pp. 1–14, 2016.

[19] P. M. T. Zaal, D. M. Pool, Q. P. Chu, M. M. van Paassen, M. Mulder, and J. A. Mulder, "Modeling Human Multimodal Perception and Control Using Genetic Maximum Likelihood Estimation," *J. of Guidance, Control, and Dynamics*, vol. 32, no. 4, pp. 1089–1099, 2009.

[20] D. T. McRuer, R. E. Magdaleno, and G. P. Moore, "A Neuromuscular Actuation System Model," *IEEE Trans. on Man-Machine Systems*, vol. 9, no. 3, pp. 61–71, 1968.

[21] L. Ljung, *System Identification Theory for the User*, 2nd ed. Prentice Hall, Inc., 1999.

[22] R. D. Luce, *Response times*. Oxford University Press, 1986, no. 8.

[23] R. M. Gottsdanker, "The Ability of Human Operators to Detect Acceleration of Target Motion," *Psychological Bulletin*, vol. 53, no. 6, pp. 477–487, 1956.

[24] F. M. Drop, R. J. De Vries, M. Mulder, and H. H. Bülthoff, "The Predictability of a Target Signal Affects Manual Feedforward Control," in *Proc. of the 13th IFAC/IFIP/IFORS/IEA Symposium on Human-Machine Systems*, 2016, pp. 177–182.

[25] M. Mulder, D. M. Pool, D. A. Abbink, E. R. Boer, P. M. T. Zaal, F. M. Drop, K. van der El, and M. M. van Paassen, "Manual Control Cybernetics: State-of-the-Art and Current Trends," *IEEE Transactions on Human-Machine Systems*, accepted 2017.

**Frank M. Drop** (M'12) received the M.Sc. and Ph.D. degrees from TU Delft, The Netherlands, in 2011 and 2016, respectively. He obtained the Ph.D. degree on feedforward manual control in the context of a collaborative project between the Faculty of Aerospace Engineering and the Department of Human Perception, Cognition and Action, Max Planck Institute for Biological Cybernetics, Tübingen, Germany. His research interests include cybernetics and modeling of human control, and is currently working on novel motion cueing algorithms based on model predictive control.

**Daan M. Pool** (M'09) received the M.Sc. and Ph.D. degrees (*cum laude*) from TU Delft, The Netherlands, in 2007 and 2012, respectively. He is currently an Assistant Professor with the section Control and Simulation, Aerospace Engineering, TU Delft. His research interests include cybernetics, manual vehicle control, simulator-based training, and mathematical modeling, identification, and optimization techniques.

**Marinus (René) M. van Paassen** (M '08; SM '15) is an associate professor in Aerospace Engineering at the Delft University of Technology, working on human machine interaction and aircraft simulation. His work on human-machine interaction ranges from studies of perceptual processes, haptics and haptic interfaces and human manual control to design of and interaction with complex cognitive systems. In the latter field, he applies cognitive systems engineering analysis (abstraction hierarchy and multi-level flow modeling) and ecological interface design to the work domain of vehicle control. René is Associate Editor for the IEEE Transactions on Human-Machine Systems.

**Max Mulder** (M 16) received the M.Sc. degree and Ph.D. degree (*cum laude*) in aerospace engineering from Delft University of Technology, Delft, The Netherlands, in 1992 and 1999, respectively, for his work on the cybernetics of tunnel-in-the-sky displays. He is currently Full Professor and Head of the Control and Simulation Division, Faculty of Aerospace Engineering, Delft University of Technology. His research interests include cybernetics and its use in modeling human perception and performance, and cognitive systems engineering and its application in the design of "ecological human-machine interfaces.

**Heinrich H. Bülthoff** is scientific member of the Max Planck Society and managing director at the Max Planck Institute for Biological Cybernetics. He is head of the Department Human Perception, Cognition and Action in which about seventy perception scientists and engineers investigate psychophysical and computational aspects of perception and cognition. For his research on man machine interfaces, he has built a state-of-the-art virtual reality facility, the Cyberneum, and two unique Motion Simulators for basic and applied research on multi-sensory perception and control. He holds a Ph.D. degree in the natural sciences from the Eberhard Karls Universität in Tübingen. He worked as research scientist at the Massachusetts Institute of Technology before becoming Professor of Cognitive Science at Brown University. He returned to Germany in 1993 as a director of the Max Planck Institute in Tübingen. He is Honorary Professor at Tübingen University and was adjunct Professor at Korea University in Seoul. He is involved in many international collaborations and a member of national and international University boards. He is initiator of the European Projects CyberWalk and myCopter and member of several European research networks.